CORE
Metadata, citation and similar papers at core.ac.uk
Provided by UPCommons. Portal del coneixement obert de la UPC

XIV International Conference on Computational Plasticity. Fundamentals and Applications
COMPLAS XIV
E. Oñate, D.R.J. Owen, D. Peric & M. Chiumenti (Eds)

LMIT AND SHAKEDOWN ANALYSIS BASED ON SOLID SHELL MODELS

LEONARDO LEONETTI *, GIOVANNI GARCEA.* DOMENICO MAGISANO * FRANCESCO LIGUORI*

* Dipartimento di Ingegneria Informatica, Modellistica, Elettronica e Sistemistica
Universit della Calabria 87036 Rende (Cosenza), Italy
web page: http://www.labmec.unical.it/

Key words: Computational Plasticity, Shakedown, Optimization, Solid Shells

Abstract. The paper treats the formulation of the shakedown problem and, as special case, of the limit analysis problem, using solid shell models and ES-FEM discratization technology. In this proposal the Discrete shear gap method is applied to alleviate the shear locking phenomenon.

1 INTRODUCTION

Shakedown analysis plays an important role in assessing the safety of structures in presence of many independent load combinations [1] against plastic collapse, loss in functionality due to excessive deformation (ratcheting) or collapse due to low cycle fatigue.

Nowadays, due to the growing attention of the scientific community, solid-shell elements have reached a high level of efficiency and accuracy. It has been shown that solid-shell finite elements give some advantages in linear and nonlinear context of analysis [2]. When compared to shell elements, solid-shell formulations present a simpler structure since only displacement degrees-of-freedom are employed. They can automatically account for 3D constitutive relations and are able to model through the thickness behaviours more accurately without the need to resort plane-stress assumptions, which often occurs in shell elements including rotation degrees-of-freedom. Solid-shell formulations also present important advantages when considering double-sided contact situations and in treating large deformations, since no rotation degrees-of-freedom are involved. However in addition to the classical shear, membrane and volumetric lockings, in the solid-shell exhibits thickness and trapezoidal locking. The latter is typical only of low order FEM. Assumed Natural Strain, Enhanced Assumed Strain and mixed (hybrid) formulations have been proposed for resolving these locking phenomena. In the context of triangular grids, the Assumed Natural Strain doesn't solve at all the shear locking [3] and a good alternative seems to be the so-called Discrete Shear Gap method [4]. Particularly for these models, to be competitive, it is better to improve the behaviour of lower-order finite elements due to its low computational cost when moderately fine meshes are required. To this aim linear

triangular (T_3) discretization [5] is highly suitable for describing complicated data and shows little sensitivity to the mesh distortion.

In order to alleviate the overstiffness of lower order FEMs various solutions have been proposed in the literature and smoothed finite element methods (SFEM) represent a a quite recent and effective numerical strategy. It is based on the idea of defining a smoothing domain through the discretization with different patterns, i.e. cells, nodes, edges or faces of a background mesh. More recently, the smoothing concept has been extended to elements with higher order shape functions [6, 7] simply obtained by using a mixed method. For an exhaustive description of the S-FEM method and a complete list of references, the authorship can find in [8].

Obviating the need to perform a cumbersome incremental elasto-plastic analysis [9, 10, 11], direct methods has been proved to be one of the most powerful tools to estimate the shakedown safety load of practical engineering structures.

The aim of this paper is to present a mixed shakedown (limit) analysis formulation for solid-shells. The proposed mixed element is based on a Edge Smoothed representation of the displacement field and piece-wise constant description of the stress field. The mixed nature of the element gives coherent equilibrium equations suitable for the simple application to the shakedown analysis and prevents volumetric locking problem. The assumed piece-wise constant description of the stress field allows the discontinuities inherent in the plastic solution. Furthermore, the model is particularly simple and easy to implement while providing accurate solutions of the plastic collapse analysis. Among other benefits the proposed MES-FEM model resolves also the dependency of state-of-art triangular solid shell elements on the adaptation of the cross-diagonal mesh. It is constructed by using a mixed format as described in [6, 7], and is suitable to perform well also in geometrically nonlinear context [12, 2, 13].

The yield criteria are borrowed from classical shell shear deformable shell models rewritten in terms of the variables used in defining the solid shell model used.

Another FEM model based on the so-called composite concept [14, 15, 16] is derived and compared with the ES-FEM ancestor.

2 THE SOLID-SHELL FINITE ELEMENT

In this section we briefly recall the kinematics of solid-shell finite element following the description of Sze et al. [17, 3].

2.1 Kinematics in convective frame

The convective coordinates $\zeta = \{\xi, \eta, \zeta\}$ are used to express the FE interpolation. A position vector in the initial or current configuration are denoted by $\mathbf{X}[\zeta] \equiv \{\mathbf{X_1}[\zeta], \mathbf{X_2}[\zeta], \mathbf{X_3}[\zeta]\}$ and $\mathbf{Y}[\zeta] \equiv \{\mathbf{Y_1}[\zeta], \mathbf{Y_2}[\zeta], \mathbf{Y_3}[\zeta]\}$ respectively and are linked by the displacement field $\mathbf{d}[\zeta]$

$$\mathbf{Y}[\zeta] = \mathbf{X}[\zeta] + \mathbf{d}[\zeta] \tag{1}$$

Adopting the convention of summing on repeated indexes, the covariant Green-Lagrange

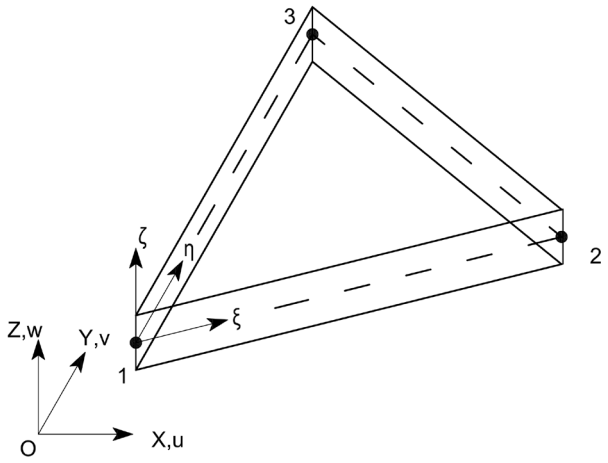

Figure 1: Linear triangular based solid-shell element

strain measure components are

$$\bar{\varepsilon}_{ij} = \frac{1}{2}\left(\mathbf{X}_{,\mathbf{i}}\cdot\mathbf{d}_{,\mathbf{j}} + \mathbf{d}_{,\mathbf{i}}\cdot\mathbf{X}_{,\mathbf{j}} + \mathbf{d}_{,\mathbf{i}}\cdot\mathbf{d}_{,\mathbf{j}}\right) \quad \text{with} \quad i,j = \xi,\eta,\zeta \tag{2}$$

where a comma followed by k denotes the derivative with respect to kth component of ζ and $(\cdot)$ denotes the scalar product.

The shell, with constant thickness, is conveniently described using a bi-dimensional frame

$$\mathbf{X}[\zeta] = \mathbf{X_0}[\xi,\eta] + \zeta\mathbf{X_n}[\xi,\eta] = \mathbf{N_d}[\zeta]\mathbf{X_e}, \qquad \mathbf{d}[\zeta] = \mathbf{d_0}[\xi,\eta] + \zeta\mathbf{d_n}[\xi,\eta] = \mathbf{N_d}[\zeta]\mathbf{d_e} \tag{3}$$

where vectors $\mathbf{d_e}$ and $\mathbf{X_e}$ collect the element nodal displacements and coordinates. The matrix $\mathbf{N_d}[\zeta]$ collects the interpolation functions

$$\mathbf{N_d}[\zeta] \equiv \left[\mathbf{N}, \zeta\mathbf{N}\right] = \mathbf{N_{d0}} + \zeta\mathbf{N_{dn}} \tag{4}$$

where $\zeta \in [-1,+1]$, $\mathbf{N_{d0}} = [\mathbf{N}[\mathbf{r},\xi,\eta], \mathbf{0}]$ and $\mathbf{N_{dn}} = [\mathbf{0}, \mathbf{N}[\mathbf{r},\xi,\eta]]$ that for linear triangular grids, the bi-dimensional shape functions $\mathbf{N} \equiv \left[N_1, \quad N_2, \quad N_3\right]$ are as usual

$$N_1 = r = 1 - \xi - \eta, \;\; N_2 = \xi, \;\; N_3 = \eta \tag{5}$$

Adopting a Voigt notation the infinitesimal covariant strain components in Eq.(2) are collected in vector $\bar{\varepsilon} \equiv [\bar{\varepsilon}_{\xi\xi}, \bar{\varepsilon}_{\eta\eta}, 2\bar{\varepsilon}_{\xi\eta}, \bar{\varepsilon}_{\zeta\zeta}, 2\bar{\varepsilon}_{\eta\zeta}, 2\bar{\varepsilon}_{\xi\zeta}]^T$ that, exploiting Eq.(3), becomes

$$\bar{\varepsilon} \equiv \begin{bmatrix} \mathbf{X_e^T}\mathbf{N_{d,\xi}^T}\mathbf{N_{d,\xi}} \\ \mathbf{X_e^T}\mathbf{N_{d,\eta}^T}\mathbf{N_{d,\eta}} \\ \mathbf{X_e^T}(\mathbf{N_{d,\xi}^T}\mathbf{N_{d,\eta}} + \mathbf{N_{d,\eta}^T}\mathbf{N_{d,\xi}}) \\ \mathbf{X_e^T}\mathbf{N_{d,\zeta}^T}\mathbf{N_{d,\zeta}} \\ \mathbf{X_e^T}(\mathbf{N_{d,\zeta}^T}\mathbf{N_{d,\eta}} + \mathbf{N_{d,\eta}^T}\mathbf{N_{d,\zeta}}) \\ \mathbf{X_e^T}(\mathbf{N_{d,\xi}^T}\mathbf{N_{d,\zeta}} + \mathbf{N_{d,\zeta}^T}\mathbf{N_{d,\xi}}) \end{bmatrix} \mathbf{d_e}, \tag{6}$$

The covariant strains can be conveniently linearized with respect to ζ in the following form

$$\bar{\varepsilon} \approx \begin{bmatrix} \bar{\mathbf{e}}[\xi,\eta] + \zeta\ \bar{\chi}[\xi,\eta] \\ \bar{\varepsilon}_{\zeta\zeta}[\xi,\eta] \\ \bar{\boldsymbol{\gamma}}[\xi,\eta] \end{bmatrix} \tag{7}$$

and collected in the vector $\bar{\rho}[\zeta] = \bar{\rho}[\xi,\eta] \equiv [\bar{\mathbf{e}}, \bar{\varepsilon}_{\zeta\zeta}, \bar{\chi}, \bar{\boldsymbol{\gamma}}]^T$

where

$$\bar{\mathbf{e}}[\xi,\eta] \equiv \begin{bmatrix} \bar{\varepsilon}_{\xi\xi} \\ \bar{\varepsilon}_{\eta\eta} \\ 2\bar{\varepsilon}_{\xi\eta} \end{bmatrix} \quad \bar{\chi}[\xi,\eta] \equiv \begin{bmatrix} \bar{\varepsilon}_{\xi\xi,\zeta} \\ \bar{\varepsilon}_{\eta\eta,\zeta} \\ 2\bar{\varepsilon}_{\xi\eta,\zeta} \end{bmatrix} \quad \bar{\boldsymbol{\gamma}}[\xi,\eta] \equiv \begin{bmatrix} 2\bar{\varepsilon}_{\eta\zeta} \\ 2\bar{\varepsilon}_{\xi\zeta} \end{bmatrix}$$

By partitioning the vectors $\mathbf{d_e} = [\mathbf{d_{0e}}, \mathbf{d_{en}}]^{\mathbf{T}}$ and $\mathbf{d_e} = [\mathbf{X_{e0}}, \mathbf{X_{ne}}]^{\mathbf{T}}$ the components of generalized covariant strains (7) have the following form

$$\begin{aligned} \bar{\mathbf{e}}_1 &= \mathbf{X_e^T Q^m_{\xi\xi} d_e},\ \bar{\mathbf{e}}_2 = \mathbf{X_e^T Q^m_{\eta\eta} d_e},\ \bar{\mathbf{e}}_3 = \mathbf{X_e^T Q^m_{\xi\eta} d_e} \\ \bar{\chi}_1 &= \mathbf{X_e^T Q^b_{\xi\xi} d_e},\ \bar{\chi}_2 = \mathbf{X_e^T Q^b_{\eta\eta} d_e},\ \bar{\chi}_1 = \mathbf{X_e^T Q^b_{\xi\eta} d_e} \\ \bar{\varepsilon}_{\zeta\zeta} &= \mathbf{X_e^T Q_{\zeta\zeta} d_e},\ 2\bar{\varepsilon}_{\xi\zeta} = \mathbf{X_e^T Q_{\xi\zeta} d_e},\ 2\bar{\varepsilon}_{\eta\zeta} = \mathbf{X_e^T Q_{\eta\zeta} d_e} \end{aligned} \tag{8}$$

It can be shown that the operators involved in previous equations are of compact shape.

2.2 Remedies for shear and trapeziodal locking

A way of resolving shear locking is the Assumed Natural Strain method in which the natural transverse shear strains are sampled at some discrete element points and then interpolated. As shown in [3, 18] also after this treatment triangular elements based on ANS still have a moderate chance of exhibiting shear locking.

The so-called Discrete Shear Gap method [4] that can be classified as an ANS method is another effective strategy of resolving shear locking gives some advantage. The element formulation is automatic for any kind of element, regardless of shape and polynomial order, there is no need to choose an interpolation for the shear strains or to specify any sampling points. The process to construct DSG is similar for both triangles and quadrangles whereas in applying the ANS to triangles a proper choice of feasible sampling points proves to be more problematic than for rectangles [4].

The DSG algorithm is employed in this finite element formulation

- Evaluation of the discrete shear gaps by integrating the transverse shear strains, or equivalently the corresponding matrices $\mathbf{Q}$s (8)

$$\begin{aligned} \Delta\gamma^1_{\xi z} = 0,\ \ \Delta\gamma^2_{\xi z} = \int_{\xi_1}^{\xi_2} \bar{\mathbf{Q}}_{\xi\zeta} d\xi,\quad \Delta\gamma^3_{\xi z} = \int_{\xi_1}^{\xi_3} \bar{\mathbf{Q}}_{\xi\zeta} d\xi \\ \Delta\gamma^1_{\eta z} = 0,\ \ \Delta\gamma^2_{\eta z} = \int_{\eta_1}^{\eta_2} \bar{\mathbf{Q}}_{\eta\zeta} d\eta,\quad \Delta\gamma^3_{\eta z} = \int_{\eta_1}^{\eta_3} \bar{\mathbf{Q}}_{\eta\zeta} d\eta \end{aligned} \tag{9}$$

  $\bar{\mathbf{Q}}_{\xi\zeta}$ and $\bar{\mathbf{Q}}_{\eta\zeta}$ are obtained from compatibility relations (3). It is worth mentioning that these integrals are carried out apriori analitically

- Interpolation of the discrete shear gaps across the element in order to obtain the suitable discrete form

$$\begin{aligned}\mathbf{Q}_{\xi\zeta} &= \frac{\partial \mathbf{N_2}}{\partial \xi}\boldsymbol{\Delta}\gamma^{\mathbf{2}}_{\xi\mathbf{z}} + \frac{\partial \mathbf{N_3}}{\partial \xi}\boldsymbol{\Delta}\gamma^{\mathbf{3}}_{\xi\mathbf{z}} \\ \mathbf{Q}_{\eta\zeta} &= \frac{\partial \mathbf{N_2}}{\partial \eta}\boldsymbol{\Delta}\gamma^{\mathbf{2}}_{\eta\mathbf{z}} + \frac{\partial \mathbf{N_3}}{\partial \eta}\boldsymbol{\Delta}\gamma^{\mathbf{3}}_{\eta\mathbf{z}}\end{aligned} \tag{10}$$

Similarly to shear locking, the excessive number of sampled thickness strains lead to trapezoidal locking. It can be reduced in the system level by sampling the strain along the element edges [19], namely

$$\mathbf{Q}_{\zeta\zeta} = \mathbf{r}\bar{\mathbf{Q}}\big|_{\boldsymbol{\xi}=\mathbf{0},\eta=\mathbf{0}} + \xi\bar{\mathbf{Q}}\big|_{\mathbf{r}=\mathbf{0},\eta=\mathbf{0}} + \eta\bar{\mathbf{Q}}\big|_{\boldsymbol{\xi}=\mathbf{0},\mathbf{r}=\mathbf{0}} \tag{11}$$

In this way the element is free from trapezoidal locking and is immune to shear locking as the other standard three-node degenerated shell elements [18, 20]

2.3 Dual variables of generalized strain components

Once the kinematic model is assumed (or vice versa) the related stress variables are automatically given by assuring the invariance of the internal work. By collecting the contravariant stress components $\bar{\sigma} \equiv [\bar{\sigma}_{\xi\xi}, \bar{\sigma}_{\eta\eta}, 2\bar{\sigma}_{\xi\eta}, \bar{\sigma}_{\zeta\zeta}, 2\bar{\sigma}_{\eta\zeta}, 2\bar{\sigma}_{\xi\zeta}]^T$ the work conjugate variables with $\bar{\rho}$ are obtained by

$$\mathcal{W} = \int_V \bar{\varepsilon}^T \bar{\sigma} dV = \int_\Omega \left(\bar{\mathcal{N}}^T \bar{\mathbf{e}} + \bar{\mathcal{M}}^T \bar{\chi} + \bar{s}_{\zeta\zeta}\bar{\varepsilon}_{\zeta\zeta} + \bar{\mathcal{T}}^T \bar{\boldsymbol{\gamma}}\right) \tag{12}$$

The generalized contravariant stresses are then

$$\bar{\mathcal{N}} \equiv \frac{1}{2}\int_{-1}^{1} \sigma_{\mathbf{p}} \mathbf{d}\zeta \quad \bar{\mathcal{M}} \equiv \frac{1}{2}\int_{-1}^{1} \zeta\sigma_{\mathbf{p}} \mathbf{d}\zeta \quad \bar{\mathbf{s}}_{\zeta\zeta} \quad \equiv \frac{1}{2}\int_{-1}^{1} \sigma_{\zeta\zeta} d\zeta \bar{\mathcal{T}} \quad \equiv \frac{1}{2}\int_{-1}^{1} \tau \mathbf{d}\zeta \tag{13}$$

with

$$\bar{\sigma}_p = \begin{bmatrix} \bar{\sigma}_{\xi\xi} \\ \bar{\sigma}_{\eta\eta} \\ \bar{\sigma}_{\xi\eta} \end{bmatrix} \quad \bar{\tau} = \begin{bmatrix} \bar{\sigma}_{\xi\zeta} \\ \bar{\sigma}_{\eta\zeta} \end{bmatrix} \text{ and } \quad \bar{\mathbf{t}} \equiv \left[\bar{\mathcal{N}}, \bar{s}_{\zeta\zeta}, \bar{\mathcal{M}}, \bar{\mathcal{T}}\right]^T$$

The way of performing the integral $\int_\Omega(\cdots)$ defines the finite element formulation.

2.4 The mapping to physical coordinates

A physical coordinate system is used to describe the material properties that can be different for each patch (subdomain) in which the domain may be partitioned. It is assumed that $x-y$ plane is coincident with the mid-plane of the shell ($\zeta = 0$, ζ parallel to z). With these assumptions the generalized Cartesian strain and stresses are obtained from the natural ones as

$$\begin{aligned}\mathbf{t} &= \mathbf{T}_\sigma \bar{\mathbf{t}} \\ \rho &= \mathbf{T}_\epsilon \bar{\rho} = \mathbf{T}_\sigma^{-\mathbf{T}} \bar{\rho}\end{aligned} \quad \text{with} \quad \mathbf{T}_\sigma = \begin{bmatrix} \mathbf{T_p} & 0 & 0 & 0 \\ 0 & T_z & 0 & 0 \\ 0 & 0 & \mathbf{T_p} & 0 \\ 0 & 0 & 0 & \mathbf{T_t} \end{bmatrix} \tag{14}$$

where $T_z = z_{,\zeta}^2 = \frac{h^2}{4}$ and where h is the thickness of the shell and

$$\mathbf{T_p} = \begin{bmatrix} x_{,\xi}^2 & y_{,\eta}^2 & 2x_{,\xi}x_{,\eta} \\ y_{,\xi}^2 & y_{,\eta}^2 & 2y_{,\xi}y_{,\eta} \\ x_{,\xi}y_{,\xi} & x_{,\eta}y_{,\eta} & x_{,\xi}y_{,\eta} + x_{,\eta}y_{,\xi} \end{bmatrix} \qquad \mathbf{T_t} = z_{,\zeta} \begin{bmatrix} x_{,\xi} & x_{,\eta} \\ y_{,\xi} & y_{,\eta} \end{bmatrix} \tag{15}$$

and $\mathbf{x}_\xi = \mathbf{R}\mathbf{X_0}_{,\xi}$, $\mathbf{x}_\eta = \mathbf{R}\mathbf{X_0}_{,\eta}$. The matrix $\mathbf{R} = [\boldsymbol{i}_x^T, \boldsymbol{i}_y^T, \boldsymbol{i}_z^T]^T$ collects by row the unit vectors along the axis of the local Cartesian coordinates

$$\boldsymbol{i}_x = \frac{\mathbf{X_0}_{,\xi}}{\|\mathbf{X_0}_{,\xi}\|} \text{ or provided as input,} \quad \boldsymbol{i}_y = \frac{\mathbf{X_0}_{,\eta}}{\|\mathbf{X_0}_{,\eta}\|}, \quad \boldsymbol{i}_z = \boldsymbol{i}_x \times \boldsymbol{i}_y$$

Being the Jacobian matrix $\mathbf{J}$

$$\mathbf{J_0}[\xi, \eta] = \begin{bmatrix} \mathbf{X_0}_{,\xi} & \mathbf{X_0}_{,\eta} & \mathbf{X_0}_{,\zeta} \end{bmatrix} = \begin{bmatrix} x_{,\xi} & y_{,\xi} & 0 \\ x_{,\eta} & y_{,\eta} & 0 \\ 0 & 0 & h/2 \end{bmatrix} \tag{16}$$

constant with ζ its determinant can be evaluated as $det(\mathbf{J}) = \mathbf{Ah}$ where $2A = x_{,\xi}y_{,\eta} - y_{,\xi}x_{,\eta}$

2.5 Edge smoothed element topology

The solid shell model is based on a description of a bi-dimensional domain using three-dimensional strain measure. Many advantages in employing Smoothed FEM (S-FEM) have been proven [8, 21] but standard formulation still show some drawback. Is the authors opinion that the generation of the mesh for S-FEM-type elements, including edge imbricate FEM (EI-FEM) [22] is not trivial. Recently in [23] a nice method for an automatic mesh generation for S-FEM have been developed. It is also the authors opinion also that the simplest, automatic and costless way to describe the S-FEM models based on first order grids (T_3 or Q_4) is to use a quadratic grids and stress assumption [6] instead of strain assumptions. In this way the method can be easily generalized to higher shape functions and the preprocessing is simple.

Similarly to ES-FEM, we start from a geometrical discretization of the two-dimensional domain (*grid*), by means of three node triangles (*parts*). Each part can be subdivided into three triangular *subparts* identified by each edge and the centroid of the part. On this grid the *element* is defined by the union of the subparts adjacent to each edge of the grid (see [6]). The union of all the elements defines the *mesh*. Each part contributes to the elements corresponding to its sides, so the mesh (of the elements) is not coincident with the grid (of the parts).

To obtain the numerical model in each part the stress components are collected as $\mathbf{t}_e = [\mathbf{t}_e^1, \mathbf{t}_e^3, \mathbf{t}_e^3]$ with $\mathbf{t}^i = \left[\mathcal{N}^\mathbf{i}, \mathbf{s}_{\zeta\zeta}^\mathbf{i}, \mathcal{M}^\mathbf{i}, \mathcal{T}^\mathbf{i}\right]^T$, where superscripts denote each triangle subpart, and the displacement parameters are collected as

$$\mathbf{d_e} = [\mathbf{u_1}...\mathbf{u_3}, \mathbf{v_1}...\mathbf{v_3}, \mathbf{w_1}...\mathbf{w_3}, \mathbf{u_{n1}}..., \mathbf{u_{n3}}, \mathbf{v_{n1}}..., \mathbf{v_{n3}}, \mathbf{w_{n1}}..., \mathbf{w_{n3}}]^\mathbf{T} \tag{17}$$

where subscripts $1, 2, 3$ denote the vertex of the triangular part. With the same shape is assumed the vector $\mathbf{X_e}$

3 CONSTITUTIVE EQUATIONS AND YIELD CRITERIA

The perfectly-plastic material assumption restrains the stress σ to belong to a fix admissible domain

$$\mathbb{E} \equiv \{\sigma : \mathbf{f}[\sigma] \leq \mathbf{0}, \text{with} \mathbf{f}[\mathbf{0}] < \mathbf{0}\} \tag{18}$$

where the function $f[\sigma]$ is a convex yield function. Exploiting its convexity the constitutive relation follows

$$\dot{\varepsilon^{\mathbf{p}}} = \dot{\mu} \frac{\partial f[\sigma]}{\partial \sigma} \Big|_{f(\sigma)=\mathbf{0}} \tag{19}$$

due to Drucker condition

$$(\sigma_{\mathbf{y}} - \sigma)^{\mathbf{T}} \dot{\varepsilon}^{\mathbf{p}} \geq \mathbf{0} \quad \forall \sigma \in \mathbb{E}$$

3.1 Von Mises yield criterion

The classical H. V. Mises yield criterion for metal shells, generalized in terms of stress resultants (13) can be expressed as [24]

$$\frac{1}{2} \mathbf{t}^T \mathbf{P_e} \mathbf{t} \leq \sigma_{\mathbf{y}}^{\mathbf{2}} \tag{20}$$

where

$$\mathbf{P_e} = \begin{bmatrix} 2 & -1 & \cdot & -1 & \cdot & \cdot & \cdot & \cdot & \cdot \\ -1 & 2 & \cdot & -1 & \cdot & \cdot & \cdot & \cdot & \cdot \\ \cdot & \cdot & 6 & \cdot & \cdot & \cdot & \cdot & \cdot & \cdot \\ -1 & -1 & \cdot & 2 & \cdot & \cdot & \cdot & \cdot & \cdot \\ \cdot & \cdot & \cdot & \cdot & 2h^2 & -h^2 & \cdot & \cdot & \cdot \\ \cdot & \cdot & \cdot & \cdot & -h^2 & 2h^2 & \cdot & \cdot & \cdot \\ \cdot & \cdot & \cdot & \cdot & \cdot & \cdot & 6h^2 & \cdot & \cdot \\ \cdot & \cdot & \cdot & \cdot & \cdot & \cdot & \cdot & \frac{3h^2}{2} & \cdot \\ \cdot & \cdot & \cdot & \cdot & \cdot & \cdot & \cdot & \cdot & \frac{3h^2}{2} \end{bmatrix}, \tag{21}$$

Note that the terms of $\frac{3h^2}{2}$ in the matrix $\mathbf{P}$ are the transverse shear components.

4 SHAKEDOWN ANALYISIS

We refer to the analysis of a body subjected to volume forces $\partial\Omega$ and tractions $\mathbf{f}$, both increasing with the same load multiplier λ.

The proncipal virtual work equation becomes

$$W[\sigma, \mathbf{u}] = \int_{\Omega} \sigma^{\mathbf{T}} \mathbf{D} \mathbf{u} \, \mathbf{d\Omega} - \int_{\mathbf{\Omega}} \mathbf{b}^{\mathbf{T}} \mathbf{u} \, \mathbf{d\Omega} - \int_{\mathbf{\Gamma}}^{\mathbf{T}} \mathbf{u} \, \mathbf{d\Gamma} \tag{22}$$

where $\mathbf{D}$ is the compatibility operator. By introducing the interpolation the part contribution to the

$$W_e[\boldsymbol{\beta}_e, \mathbf{d_e}] = \boldsymbol{\beta}_{\mathbf{e}}^{\mathbf{T}} \mathbf{D_e} \mathbf{d_e} - \mathbf{d}_{\mathbf{e}}^{\mathbf{T}} \mathbf{p_e} \tag{23}$$

and $\mathbf{D_e}$ is the discrete compatibility operator, $\mathbf{p_e}$ is the load vector furnished by the integration of the external load components weighted with the shape functions of the displacement interpolations.

The global compatibility operator $\mathbf{Q}$ and load vector $\mathbf{p}$ are obtained by assembling the element contributions through the element incidence operators for displacements $\mathbf{u_e} = \mathbf{T_u q}$ and stresses $\boldsymbol{\beta}_e = \mathbf{T}_\beta \boldsymbol{\beta}$, where $\boldsymbol{\beta}$ is the global stress vector and $\mathbf{q}$ is the global displacement vector.

The material is assumed to be elastic-perfectly plastic, therefore the stress field is constrained to satisfy plastic admissibility inequalities which are independent of the plastic strain. The shakedown analysis can be solved using an evolutive analysis through the solution of a sequence of incremental elasto-plastic problems [9] and the shakedown multiplier λ_s is evaluated as the limit value for the equilibrium path. The shakedown analysis theorems offer an alternative way which is directly addressed to compute the lower and upper approximations of the safety multiplier. In this case, following [9] the shakedown multiplier is individuated as a solution of the nonlinear mathematical programming problem

$$\begin{aligned} &\text{maximize} && \lambda \\ &\text{subject to} && \mathbf{Q^T}\boldsymbol{\beta} - \lambda \mathbf{p} = \mathbf{0} \\ & && \phi[\boldsymbol{\beta}] \leq \mathbf{0} \end{aligned} \tag{24}$$

where the equality constraints are represented by the equilibrium equations, described through the global equilibrium operator $\mathbf{Q^T}$ and the load vector $\mathbf{p}$ collecting the body forces and tractions. The plastic admissibility inequalities are expressed through the vector ϕ, which collects the local restrictions imposed by the assumed yield condition over the stress state $\mathbf{t}^i$ of the N_r regions of the domain

$$\phi_i[\mathbf{t}^i, \lambda] \leq 0, \quad i = 1..N_r \tag{25}$$

For more details in the formulation of the shakedown problem the reader is encouraged to see [9].

5 NUMERICAL RESULTS

The performances of the proposed mixed finite element model in evaluating plastic collapse states have been tested by the numerical experiments reported in the following subsections.

5.1 Cook membrane

The well-known Cook's membrane, depicted in Figure 2 is used to show some preliminary results of the in-plane behaviour. The convergence of the numerical solution has been tested by using three meshes obtained by successive refinements initiated by a coarse mesh of 2 elements for each side.

Table 1 reports a comparison of the computed values of the plastic collapse multiplier. The reference result [11] was obtained using a mesh having 1024 elements and 2178 dofs

while the finest mesh used in the present analysis has 512 triangular elements and 1649 dofs.

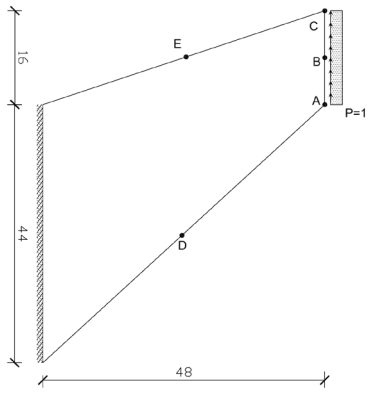

Figure 2: Cook membrane data.

Table 1: Cook membrane. Plane stress limit analysis.

	mesh 1	*mesh 2*	*mesh 3*
	λ	λ	λ
Present	0.4151	0.4012	0.3970
$N-S$	0.3888	0.3883	0.3935
ref. [11]			0.3956

5.2 Square plate under uniform transverse load

The transverse performances are tested by exercising the simply supported (SS) and clamped (CL) square plates as described in Fig. 3 subject to uniform transverse load $q = 1$. Owing to its symmetry, only a quarter of the plate is modelled with respectively 8, 12 and 16 elements for each side. To appreciate the effectiveness in resolving the shear locking, different ratios L/h are considered. A unitary yield moment $m_y = \frac{\sigma_y h^2}{4}$ is considered. The collapse multipliers are given normalized with respect the yield moment divided by qL^2 where $q = 1$ is the transversal uniform load.

Tables 2 and 3 compare the present results with those obtained in [25], showing good agreement between solutions obtained by two methods.

6 CONCLUSIONS

The paper proposes an MES-FEM solid shell element for application in shakedown and limit analysis. The model is adapt, simple and accurate, to solve the problem also

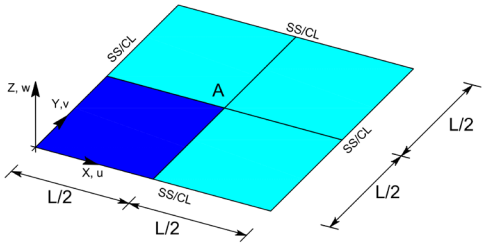

Figure 3: Square plate data. $L = 10$.

Table 2: Clamped square plate: computed plastic collapse load using uniform meshes

L/t	*mesh 1*	*mesh 2*	*mesh 3*	
	λ	λ	λ	Uniform mesh [25]
1	9.29	9.09	9.00	9.02
4	32.03	31.11	30.64	31.46
10	44.81	43.16	42.37	43.37
40	49.43	47.35	46.41	46.57
50	49.69	47.50	46.54	-
100	50.73	47.90	46.78	46.84

in conic formulation of mathematical programs. The main features of the model are its simplicity and easy implementation within existing computational tools. Nevertheless fully capitalizes its features in the analysis of plastic problems. The piece-wise constant description of the stress field address the discontinuities inherent in the plastic solution.

The numerical experiments show the good performance of the proposed model. It is worth noting that the model proves to be able to furnish very accurate results by employing moderately fine meshes using few variables and nonlinear constraints in the formulation of the mathematical program used to perform the analysis, and this is of great interest in technical applications.

The accurate results achieved in the evaluation of the collapse multiplier and in the description of the collapse mechanism demonstrate that the element is able to approximate well the discontinuous fields generated by the plastic behaviour without drawbacks and locking phenomena also for small thickness.

REFERENCES

[1] L. Leonetti, R. Casciaro, G. Garcea, Effective treatment of complex statical and dynamical load combinations within shakedown analysis of 3d frames, Computers AND Structures 158 (2015) 124 – 139.

[2] D. Magisano, L. Leonetti, G. Garcea, Advantages of the mixed format in geometrically nonlinear analysis of beams and shells using solid finite elements, International Journal for Numerical Methods in Engineering 109 (9).

Table 3: Simply supported square plate: computed plastic collapse load using uniform meshes

L/t	*mesh 1*	*mesh 2*	*mesh 3*	Uniform mesh [25]
	λ	λ	λ	λ
1	9.27	9.08	8.99	9.03
4	23.52	23.43	23.41	23.88
10	24.95	24.81	24.76	24.85
40	25.36	25.12	25.06	25.03
50	25.41	25.14	25.07	-
100	25.67	25.20	25.09	25.05

[3] A six-node pentagonal assumed natural strain solidshell element, Finite Elements in Analysis and Design 37 (8) (2001) 639 – 655.

[4] A unified approach for shear-locking-free triangular and rectangular shell finite elements, Computers and Structures 75 (3) (2000) 321 – 334.

[5] O. Zienkiewicz, R. Taylor, The finte element method, McGraw-Hill, 1989.

[6] L. Leonetti, G. Garcea, H. Nguyen-Xuan, A mixed edge-based smoothed finite element method (mes-fem) for elasticity, Computers and Structures 173 (2016) 123 – 138.

[7] L. Leonetti, G. Garcea, H. Nguyen-Xuan, A mixed node-based smoothed finite element method (mns-fem) for elasticity, Computer with Engineering (2017) in press.

[8] W. Zeng, G. R. Liu, Smoothed finite element methods (s-fem): An overview and recent developments, Archives of Computational Methods in Engineering (2016) 1–39.

[9] G. Garcea, L. Leonetti, A unified mathematical programming formulation of strain driven and interior point algorithms for shakedown and limit analysis, Int. J. Numer. Methods Eng.

[10] G. G. Bilotta A, Leonetti L, An algorithm for incremental elastoplastic analysis using equality constrained sequential quadratic programming, Computers and Structures.

[11] A. Bilotta, L. Leonetti, G. Garcea, Three field finite elements for the elastoplastic analysis of 2d continua 47 (2011) 1119–1130.

[12] D. Magisano, L. Leonetti, L. Garcea, How to improve efficiency and robustness of the newton method in geometrically non-linear structural problem discretized via displacement-based finite elements, Computer Methods in Applied Mechanics and Engineering 313 (2017) 986 – 1005.

[13] D. Magisano, L. Leonetti, G. Garcea, Koiter asymptotic analysis of multilayered composite structures using mixed solid-shell finite elements, Composite Structures 154 (2016) 296 – 308.

[14] L. Leonetti, M. Aristodemo, A composite mixed finite element model for plane structural problems, Finite Element Analysis and Design 94 (2015) 33–46.

[15] L. Leonetti, C. Le, Plastic collapse analysis of mindlin-reissner plates using a composite mixed finite element, International Journal for Numerical Methods in Engineering 105 (2016) 915–935.

[16] A. Bilotta, G. Garcea, L. Leonetti, A composite mixed finite element model for the elasto-plastic analysis of 3d structural problems, Finite Element Analysis and Design 113 (2016) 43–53.

[17] K. Sze, A. Ghali, Hybrid hexahedral element for solids, plates, shells and beams by selective scaling, International Journal for Numerical Methods in Engineering 36 (9) (1993) 1519–1540.

[18] A. F. Saleeb, T. Y. Chang, S. Yingyeunyong, A mixed formulation of c0-linear triangular plate/shell elementthe role of edge shear constraints, International Journal for Numerical Methods in Engineering 26 (5).

[19] K. Y. Sze, L. Q. Yao, S. Yi, A hybrid stress ans solid-shell element and its generalization for smart structure modelling. part iismart structure modelling, International Journal for Numerical Methods in Engineering 48 (4).

[20] Hybrid strain based three-node flat triangular shell elements, Finite Elements in Analysis and Design 17 (3) (1994) 169 – 203.

[21] H. Nguyen-Xuan, S. Bordas, H. Nguyen-Dang, Smooth finite element methods: convergence, accuracy and properties, International Journal for Numerical Methods in Engineering 74 (2008) 175–208.

[22] F. Cazes, G. Meschke, An edge-based imbricate finite element method (ei-fem) with full and reduced integration, Computers and Structures 106-107 (2012) 154–175.

[23] Y. Li, J. Yue, R. Niu, G. Liu, Automatic mesh generation for 3d smoothed finite element method (s-fem) based on the weaken-weak formulation, Advances in Engineering Software 99 (2016) 111 – 120.

[24] P. Papadopoulos, R. Taylor, An analysis of inelastic reissner-mindlin plates, Finite Elements Analysis and Design 10 (1991) 221–223.

[25] C. Le, A stabilized discrete shear gap finite element for adaptive limit analysis of mindlin-reissner plates, International Journal for Numerical Methods in Engineering 96 (2013) 231–246.